



City Research Online

City, University of London Institutional Repository

Citation: Ismail, N., Sa'ad, M., Ismaila, M., Zaini, M. K. A., Lim, K. S., Grattan, K. T. V., Brambilla, G., Rahman, B. M., Mohamad, H. & Ahmad, H. (2021). Biaxial 3D-Printed Inclinometer Based on Fiber Bragg Grating Technology. *IEEE Sensors Journal*, 21(17), pp. 18815-18822. doi: 10.1109/jsen.2021.3090105

This is the accepted version of the paper.

This version of the publication may differ from the final published version.

Permanent repository link: <https://openaccess.city.ac.uk/id/eprint/26387/>

Link to published version: <https://doi.org/10.1109/jsen.2021.3090105>

Copyright: City Research Online aims to make research outputs of City, University of London available to a wider audience. Copyright and Moral Rights remain with the author(s) and/or copyright holders. URLs from City Research Online may be freely distributed and linked to.

Reuse: Copies of full items can be used for personal research or study, educational, or not-for-profit purposes without prior permission or charge. Provided that the authors, title and full bibliographic details are credited, a hyperlink and/or URL is given for the original metadata page and the content is not changed in any way.

City Research Online:

<http://openaccess.city.ac.uk/>

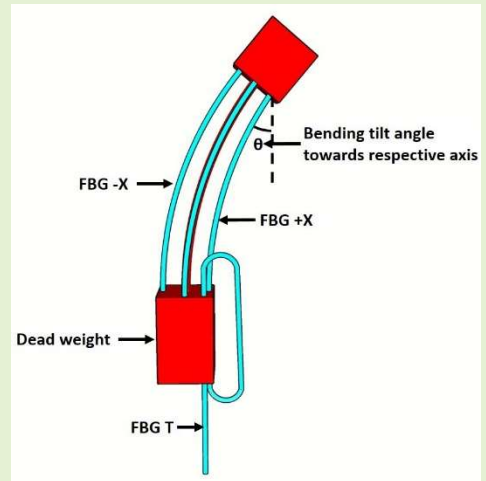
publications@city.ac.uk

Biaxial 3D-Printed Inclinometer Based on Fiber Bragg Grating Technology

N. N. Ismail, M. S. M. Sa'ad, M. F. Ismail, M. K. A. Zaini, K. S. Lim, K. T. V. Grattan, G. Brambilla, B. M. A. Rahman, H. Mohamad, and H. Ahmad

Abstract—A Fiber Bragg Grating (FBG)-based inclinometer has been developed for field use, designed to incorporate biaxial 3-dimensional (3D) printed tilt sensors (in which four FBGs were used). The inclinometer was characterized by examining its response to a wide range of tilts, over the range from 0° to 90° , towards the inclination axes. An excellent linear correlation between the wavelength shifts and the inclination angle (up to the 90° used) was obtained, showing an average sensitivity of 0.01 nm per degree of inclination angle, for each of the FBGs used. In addition to the four FBGs that form the basis of the inclination measurement, a further FBG was included in the design to allow compensation for any temperature changes experienced during the measurements. The device was calibrated over the range from -25°C to 80°C (corresponding to the extremes of cold and hot weather conditions likely to be experienced in-the-field), and a sensitivity to temperature change of $0.011\text{nm}/^\circ\text{C}$ was achieved, allowing an effective temperature correction to be applied. The data obtained from a full characterization of the performance of the sensor system, carried out in a stable, controlled environment, indicate that this inclinometer yields good sensitivity, making it highly applicable for use in monitoring rapid ground movements and deformations with its compact design allowing its wide use.

Index Terms—Inclinometer, biaxial measurements, Fiber Bragg Grating-based technology, 3D-printing, ground movements.



I. 1 INTRODUCTION

INCLINOMETERS have been widely used in various aspects of engineering and structural health monitoring, in particular to measure and characterize the inclination angles of slopes and building structures [1], as well as ground movements [2], especially those caused by heavy rainfall and floods. As an example in landslide detection, inclinometers are used in measuring the change of inclination of vertical boreholes and pipes installed in retaining structures, such as piles and diaphragms. All this allows the more accurate determination of the rate of the ground sliding direction and depth. Inclinometers in use today are typically classified into two types – probe inclinometers and in-place inclinometers. In probe inclinometers, the probe itself, (typically equipped with wheels) descends along a casing (into which grooves have been created), which is installed in a borehole [3], [4]. The probe is

then stopped at specific displacement intervals, where measurements between two specific points are obtained and used to determine the inclination angle – here measurements are usually taken manually, on-site. By contrast, for in-place inclinometers, the sensors are typically permanently installed in boreholes at pre-determined depths and positions where the ground sliding is expected to take place. The aim for such technology is that measurements can be made remotely, either at a specific time (such as after heavy rainfall) or continuously [5] as part of an early warning detection system of a possible landslide event.

In conventional electrical-based inclinometers, the variation of the inclination angles can be measured by monitoring the changes in the electrical signal caused by a magnetic effect in the sensor [6]. However, the presence of high voltages or high electromagnetic interference (such as from nearby power lines or broadcasting transmitters, for example) can affect the

This work was supported by a Newton Fund Impact Scheme, grant, ID IF022-2020, under the Newton-Ungku Omar Fund partnership. The grant is funded by the UK Department for Business, Energy and Industrial Strategy and Malaysian Industry-Government Group for High Technology (MIGHT) and delivered by the British Council and MIGHT. This work was also supported by the University of Malaya (RK021-2019 and TOP100PRC). (Corresponding author: Harith Ahmad).

N. N. Ismail, M. S. M. Sa'ad, M. F. Ismail, M. K. A. Zaini, K. S. Lim, and H. Ahmad are with the Photonics Research Center, University of Malaya, 50603 Kuala Lumpur, Malaysia. H. Ahmad also affiliated with

the Physics Dept. Faculty of Science, University of Malaya, 50603 Kuala Lumpur, Malaysia (e-mail: harith@um.edu.my).

K. T. V. Grattan and B. M. A. Rahman are with the School of Mathematics, Computer Science & Engineering, City, University of London, London, EC1V 0HB United Kingdom.

G. Brambilla is from the Optoelectronics Research Centre, University of Southampton, Southampton SO17 1BJ, United Kingdom.

H. Mohamad is with the Department of Civil and Environmental Engineering, Universiti Teknologi Petronas, Perak, Malaysia.

performance and accuracy of these sensors [7], and thus limit their use in these types of environments where often they are particularly needed. Recently, optical fiber-based sensors have become an increasingly popular alternative to conventional mechanical and electrical sensors, when configured for inclinometer applications. Over the years, various types of optical fiber based sensors have been utilized in a wide variety of civil and structural engineering, such as Fabry-Perot strain sensors [8], Michelson interferometer sensors [9], Brillouin scatter-based distributed sensors [10], [11] and Fiber Bragg Grating (FBG) sensors [12]–[19], often applied to structural or infrastructure monitoring. Since the development of FBGs [20], their lightweight nature and potential for multiplexing, as well as their use over long distances [21] are seen to suit inclinometer applications very well.

Prior research has made progress with the development of a number of different devices, but as yet there are limitations. A 2-dimensional (2D) temperature-insensitive FBG tilt sensor was demonstrated by Bao et al. in [22] where four FBGs were aligned in parallel on the outer part of a cylindrical surface, at an equal distance from each other. An accuracy of 0.2° with a resolution of 0.013° was obtained, within the limited range of -40° to 40° , towards the x-z and the y-z planes. In the work of He et al. [14], a tilt sensor with three incorporated FBGs was used to minimize the friction, rotations, and instabilities induced by their design. The FBGs (at an equal distance from each other) were suspended from a circular top plate, with a 200g weight at the bottom, but tilted only over the -15° to 15° range with respect to their axes. A further tilt sensor design, incorporating three FBGs has also been reported by Dong et al. [23], using a 2D tilt sensor design with strain-chirped FBGs, based on a vertical pendulum structure that creates a variation of the observed optical power, over the tilt angles studied. In this design, each FBG was laid on top of a small rectangular steel plate, placed onto a circular base plate and then hung on a vertical pendulum. However, a weakness is that errors in the measurements will develop with time, as the optical power may fluctuate. A problem with the designs reported above is that while they have been reported to work well in the laboratory (and thus under controlled conditions), most of them are large in size and have small operating degrees of inclination angle. This will make them less well suited to the in-the-field monitoring that is essential for a device of this type, for ground movement monitoring and a driver of this work.

Addressing the limitations in the previously reported research, this paper introduces a different design of inclinometer, based on compact tilt sensors and incorporating four FBGs for biaxial strain measurements, operating within the important -90° to 90° of tilt angle (towards the x and y axes). Care has been taken to create a design where the operating range has been extended from what has been reported above, so that it can detect tilts in any direction along the x and y axes. It was seen as critically important in the design for effective in-the-field use to provide scope for temperature compensation inside the inclinometer, so in addition to the four FBGs used for the tilt measurement itself, a further FBG was characterized in a laboratory test chamber over the temperature range, -25°C to 80°C . This inclinometer design has been created at the outset to be compact and having a wider operating range of inclination angle (-90° to 90°) towards the respective axes, in that way to

offer a practical solution for slope and structural monitoring in typical situations experienced in-the-field. Table 1 shows the comparison between the previous works and our work in terms of measurement range, sensitivity, accuracy, and resolution. Our proposed inclinometer covers a larger measurement range despite its compact design but exhibits reasonable sensitivity as compared to the other. The compact form factor enables it to be applied in such small and tight areas.

TABLE I

TABLE OF COMPARISON BETWEEN THE PREVIOUS WORKS AND OUR DESIGN IN TERMS OF ITS MEASUREMENT RANGE, SENSITIVITY, ACCURACY AND RESOLUTION

Ref.	Measurement Range	Sensitivity (nm/°)	Accuracy (°)	Resolution (nm)
[19]	-10° to 10°	0.05	3.58	0.0005
[16]	-20° to 20°	0.054	0.27	0.01
[22]	-40° to 40°	0.096	0.20	0.001
[14]	-12° to 12°	0.192	0.10	0.001
This work	-90° to 90°	0.01	0.38	0.02

II. DESIGN AND OPERATING PRINCIPLE OF THE FBG-BASED INCLINOMETER

The key elements of the design structure of this inclinometer, was based on integrated tilt sensors, as shown in Fig. 1 where the bending towards the inclination angle, causes strains which can be monitored by the FBGs integrated within the device.

The FBGs used both for tilt and temperature measurement were inscribed in the core of a hydrogenated single mode fiber by use of the phase mask technique, with a Krypton Fluoride (KrF*) excimer laser operating at a wavelength of 248 nm. Strain and temperature will affect the Bragg wavelength through the contraction or expansion of the grating pitch, where the Bragg wavelength, λ_B , of uniform FBG written in the SMF used is given by:

$$\lambda_B = 2n_{eff}\Lambda \quad (1)$$

where n_{eff} is the effective refractive index of the guided mode inside a single mode fiber and Λ is the grating pitch. When the gratings were exposed to the external perturbations (such as the strain or temperature effects here), the Bragg wavelength changes accordingly, and (1) can be rewritten as follows:

$$\frac{\Delta\lambda_B}{\lambda_B} = K_\epsilon\Delta\epsilon + K_T\Delta T \quad (2)$$

where $\Delta\lambda_B$ is the change of the Bragg wavelength, $\Delta\epsilon$ is the strain change, ΔT is the temperature change of the FBG sensor while K_ϵ and K_T are the strain and temperature coefficients, respectively.

The design of the tilt sensor, illustrating its compact dimensions, is as shown in Fig. 1(b) while the actual pictures of the sensor is depicted in Fig. 1(c) and (d). Four FBGs were used where each was attached to one of the four sides of the 3D-printed tilt sensor (printed with 5% infill density), representing the four inclination axes (+x, -x, +y, -y). To construct the device, the FBGs were inserted through the pre-printed holes on the tilt sensor and were glued at each end, using a strong liquid glue (Super Glue, cyanoacrylate).

The wavelength shifts of each FBG were then monitored, as they can be used, when calibrated, to determine the magnitudes of tilt angles. With reference to Fig. 1(a), the tensile force, F_T

and the bend moment, B of the tilt sensor can be expressed in terms of the tilt angle, θ , as follows:

$$F_T = W \cos \theta \quad (3)$$

$$B = W \cdot L \sin \theta \quad (4)$$

where W is the weight and L is the length (as shown in Fig. 1(a)). Both the tensile force and bending moment cause the change of strain to the FBGs and this change can be expressed as:

$$\Delta \varepsilon = \frac{F_T}{EA_S} \pm \frac{B}{EI_S} \quad (5)$$

where E is the elastic modulus, A_S is the cross-sectional area, and I_S is the moment of inertia of the sensor shaft. Based on (3) and (4), the change of the strain due to the inclination can be expressed as:

$$\Delta \varepsilon = \frac{W}{E} \left(\frac{\cos \theta}{A_S} \pm \frac{L \sin \theta}{I_S} \right) \quad (6)$$

As shown in Fig. 1(b), another FBG (denoted as FBG T and with a Bragg wavelength of 1558.36 nm at room temperature), was spliced to the FBG on the +x axis, glued to an adjacent pre-printed hole and was left hanging (to ensure strain insensitivity)

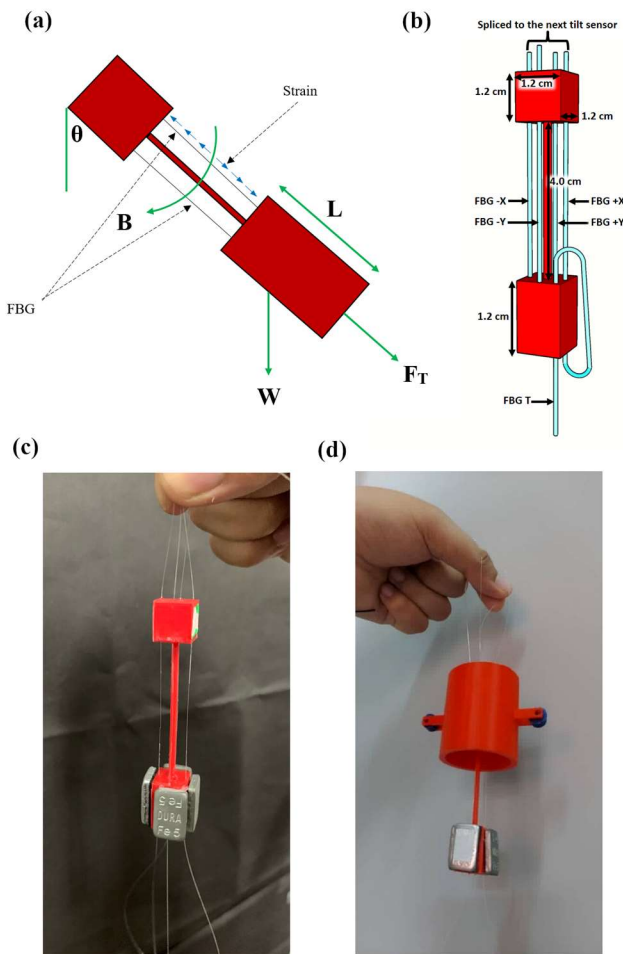


Fig. 1. Illustration of (a) the tilt sensor experiencing a tilt at an angle, (b) the tilt sensor dimensions with the incorporated FBGs at 0° inclination angle, (c) the picture of the 3D-printed sensor incorporated with FBGs, alongside four 5g weight attached to the bottom part of the sensor and (d) the 3D-printed sensor attached to its top cover with wheels as depicted in Fig. 2(c).

and thus to provide a mean for temperature compensation for the device when the temperature of operation changes.

This FBG-based in-place inclinometer was designed to be installed in a standard inclinometer casing, having an inner diameter and thickness of 70 mm and 5 mm respectively. This casing has four longitudinal wheel-grooves (labelled as 1, 2, 3, and 4), spaced 90° apart, as shown in Fig. 2(a). The inclinometer consists of three built-in tilt sensors (T1, T2, and T3) set at 30 cm intervals, connected to each other by a bendable polyvinyl chloride tube as illustrated in Fig. 2(b), where each tilt sensor (T1, T2, and T3) is installed with four FBGs, placed on four different axes (+x, -x, +y and -y) as depicted in Fig. 1(b). Each sensor is meant to determine the tilt angle at a specific measurement point. Hence this would enable the inclinometer to measure the tilt angle at three locations along with the inclinometer casing. The distance between the sensors or measurement points will be determined by the length of the tube connecting them. Each tilt sensor of this inclinometer was equipped with two units of spring-pressured wheels, positioned at points 1 and 3 of the casing to guide the inclinometer sensor along the longitudinal grooves of the casing, as depicted in Fig. 2(c). The FBGs at the +x axis (T1, T2 and T3) were spliced together in series. In addition, FBG T was also spliced to the end of the FBG at T3, in series, creating a single output from the +x axis with the four different wavelength peaks due to four different FBGs spliced then being seen. The same method was applied to the other three axes (-x, +y and -y), providing in total the four different outputs which were then recorded. The inclinometer in this way can measure the internal movement of the slope being monitored, as the device interacts closely with the surrounding soil mass and in that way allows the inclination to be recorded.

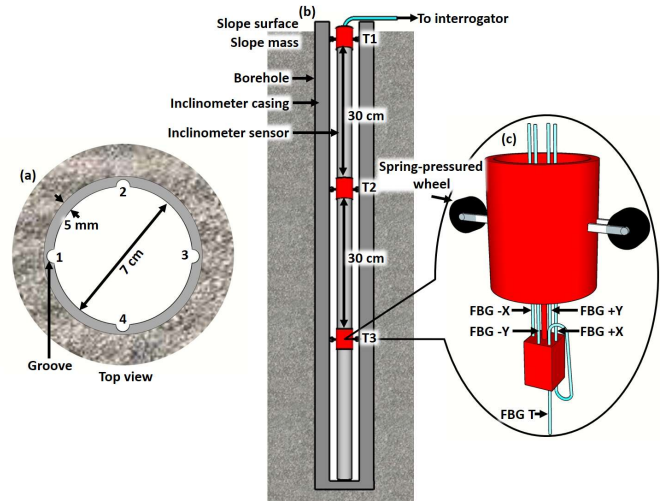


Fig. 2. Schematic design of the FBG-based inclinometer showing (a) top view of the standard inclinometer casing, (b) longitudinal section of the in-place inclinometer, and (c) built-in tilt sensor.

A. Laboratory Calibration Testing of FBG-Based Inclinometer

In this experiment, λ_B from the FBGs were observed and recorded using a Yokogawa AQ6370C Optical Spectrum Analyzer (OSA). A schematic diagram of the experimental setup is shown in Fig. 3(a), where four outputs from the inclinometer were connected to the input channels of an optical switch, while the output channel was connected to Port 2 of an

optical circulator. Port 1 and Port 3 of the circulator were coupled to an amplified spontaneous emission light source and the optical spectrum analyzer respectively. In the calibration of the inclinometer, the bottom end of the inclinometer was pushed towards each of the inclination axes depicted in Fig. 3(c): starting from an initial 0° , to 90° inclination angle, while the top end is anchored to a fixed position by a table vise, with 360° rotations used for the inclination mechanism (as illustrated in Fig. 3(b)). This procedure was repeated three times.

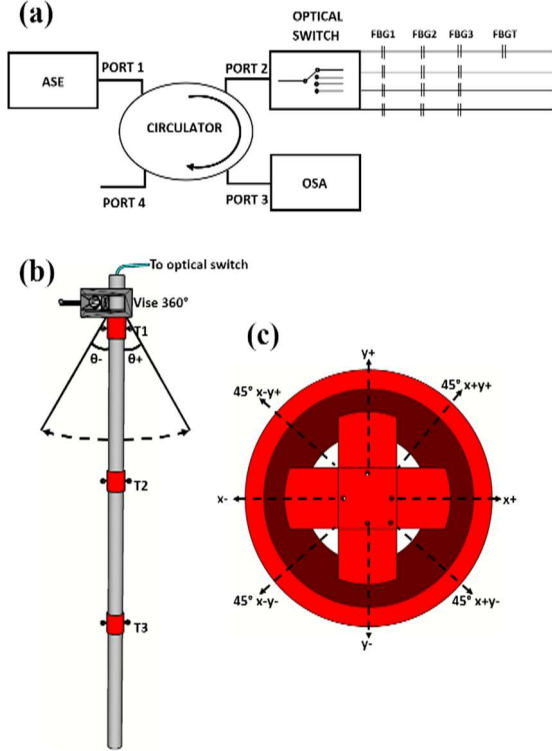


Fig. 3. Illustration of the (a) schematic diagram of the setup, (b) experimental setup, and (c) direction of the tilt (top view).

B. Calibration of the Temperature Compensation of the Inclinometer

As discussed in the previous section and expressed in (2), the FBG's Bragg wavelength, depends on the tilt angle, θ (strain) and temperature, T . It can be expressed as:

$$\lambda_B = R\theta + \lambda_{\theta=0,T} \quad (7)$$

where $\lambda_{\theta=0,T}$ is the Bragg wavelength at tilt angle, $\theta = 0$, at the temperature of T , while R is the sensitivity of the tilt sensor due to strain. $\lambda_{\theta=0,T}$ can then be expressed as:

$$\lambda_{\theta=0,T} = R_T T + \lambda_{\theta=0,T=0} \quad (8)$$

where R_T is the sensitivity of the tilt sensor due to change in temperature, and $\lambda_{\theta=0,T=0}$ is the Bragg wavelength at tilt angle, $\theta = 0$, at initial temperature.

Therefore, by considering the temperature compensation factor, the tilt angle can be expressed as:

$$\theta = \frac{\lambda_B - \lambda_{\theta=0,T}}{R} = \frac{\lambda_B - (R_T T + \lambda_{\theta=0,T=0})}{R} \quad (9)$$

To evaluate the temperature compensation over the

potentially very wide range that such a device may experience when used in-the-field, the tilt sensor was initially placed inside a polystyrene box surrounded by dry ice (solid carbon dioxide), as illustrated in Fig. 4(a), to create a stable, extreme cold environment at -25°C . The dry ice was then removed and the temperature inside the polystyrene box was allowed to rise slowly to the room temperature (of 27°C) measuring the response at 10°C intervals, through monitoring the peak wavelength shift of the FBG used (FBG T). To calibrate the device for temperatures above room temperature, the FBG was then placed in a water bath, as illustrated in Fig. 4(b) and the temperature of the water was increased from 27°C to 80°C , again with measurements of the wavelength shift being taken at intervals of 10°C . This also shows that the inclinometer is fully waterproof, an important advantage of the fiber optic device over conventional electronic-based devices. In-the-field, very wet conditions are regularly experienced when the device is used when flooding occurs, and this is a major benefit of the optical approach described here.

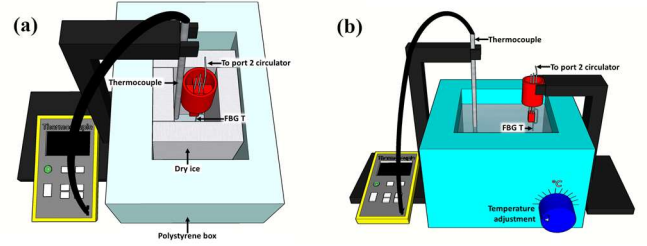


Fig. 4. Illustrations of the calibration of the device at both sub-room temperature (a) and (b) beyond room temperature. The tilt sensor was placed (a) inside a polystyrene box surrounded with dry ice to create the low temperature environment and (b) in a water bath to create the high temperature environment.

III. RESULTS AND DISCUSSION

Data from the tilt sensors, T1, T2 and T3 were collected, as indicated in Table 2, which shows the wavelengths associated with these FBGs (with their respective sensors and axes), in the experimental evaluation setup illustrated in Fig. 3. Thus Fig. 5 shows the reflective spectra of the FBGs at an initial position of a tilt angle of 0° . However, Fig. 5(a) illustrates four wavelength peaks, where there is a grating labelled as FBG T (for temperature compensation purposes) in addition to the gratings in tilt sensor T1, T2, and T3. Fig. 6 illustrates the tilt effect of the device from 0° to 90° for sensors T1, T2, and T3 as the inclinometer was tilted towards (a) the $+x$ direction (with the spectrum for FBG T for temperature compensation also included), (b) the $-x$ direction, (c) the $+y$ direction, and (d) the $-y$ direction. Specifically, Fig. 6 shows the 'redshifts' in the wavelength spectra that could be observed as the inclinometer was tilted from the initial 0° tilt to 90° , towards $+x$, $-x$, $+y$, and $-y$ directions as Figs. 6(a), (b), (c) and (d) respectively. Besides that, the insets in each subplot illustrate the response of FBG at tilt sensor T1 in greater details. The responses of other FBGs (besides the one facing the tilt direction) have also been investigated and proven to be negligible as only the FBG facing the tilt direction experienced a significant amount of strain. For instance, when the inclinometer was tilted towards the $+x$ axis, only the FBG facing $+x$ direction experienced significant strain (stress) as compared to the FBG facing $-x$, $+y$ and $-y$ directions.

Hence, there was no wavelength shift detected at the FBGs except from the one facing the tilt direction. Furthermore, in Fig. 6(a), with the same tilt angles of 0° to 90° , it was observed that all the peaks shifted to the right except for the FBG T, which indicates that it is not sensitive to strain, and thus able to provide the required temperature compensation. Fig. 7 clearly illustrates the response of the gratings at (a) +x axis, (b) -x-axis,

TABLE 2
FBG WAVELENGTHS MONITORED FOR THE DIFFERENT RESPECTIVE SENSORS AND AXES (AT AN INITIAL POSITION OF 0° INCLINATION ANGLE) AT ROOM TEMPERATURE (27°C).

Sensor	+x (nm)	-x (nm)	+y (nm)	-y (nm)
T1	1537.88	1540.90	1541.22	1539.02
T2	1546.86	1547.64	1546.94	1546.80
T3	1553.18	1553.30	1553.14	1553.54

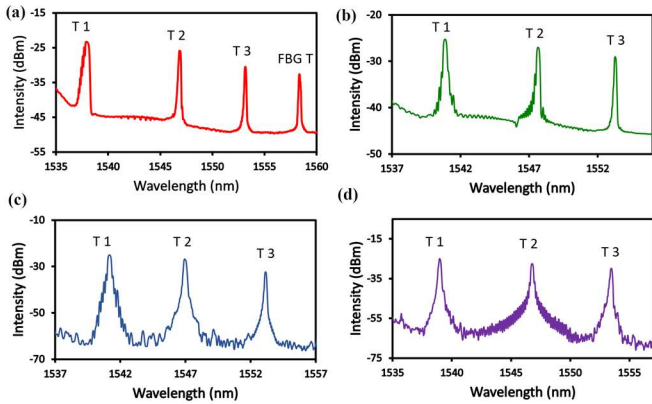


Fig. 5. Illustrations of the wavelength spectra for each tilt sensor T1, T2 and T3, at the initial position of 0° tilt angle at (a) +x direction with FBG T for temperature compensation included, (b) -x direction, (c) +y direction, and (d) -y direction at room temperature (27°C).

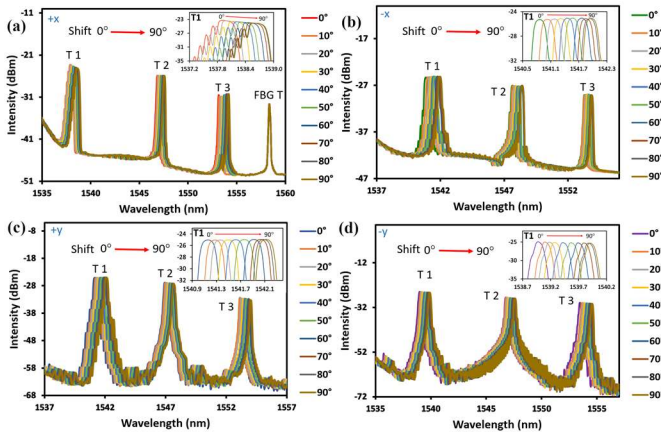


Fig. 6. Shifts of the wavelength spectra for each tilt sensor T1, T2, and T3 as the inclinometer is tilted from 0° to 90° towards (a) +x direction with FBG T for temperature compensation included, (b) -x direction, (c) +y direction, and (d) -y direction at room temperature (27°C). (insets: illustrate the expanded version of tilt sensor T1 to clearly indicate the shift, as an example.)

(c) +y axis, and (d) -y-axis for tilt sensor T1, when it is tilted from 0° to 90° towards +x direction. From this figure, we could observe that only the FBG facing the tilt direction (Fig. 7(a)) showed significant wavelength shift as compared to the FBGs at other directions (Fig. 7(b), (c), (d)) where they show zero or close to zero wavelength shift.

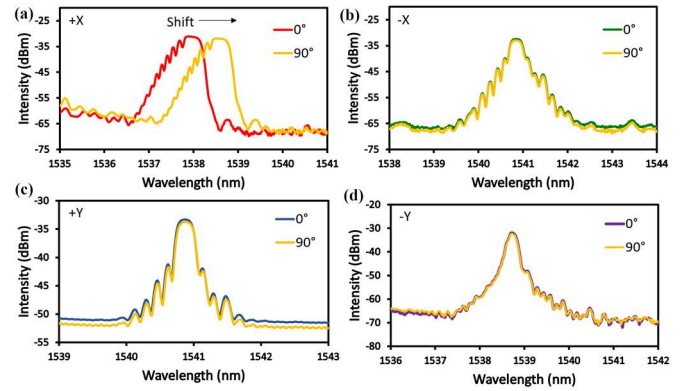


Fig. 7. The response of the gratings at (a) +x, (b) -x, (c) +y, and (d) -y-axis for tilt sensor T1 during the tilt from 0° to 90° towards +x direction at room temperature (27°C).

These results show the effectiveness of the mechanism proposed which then can be seen allows the mapping of the inclination angle – thus allowing the identification of the effects of ground movements or deformation on the tilt sensor when it is used as designed.

Further experimentation has been carried out and Fig. 8 shows the shifts of the wavelength spectra for each tilt sensor grating, T1, T2 and T3, as the inclinometer is tilted from 0° to 90° towards 45° between the (a) +x+y direction and (b) -x-y direction. Thus in Fig. 8(a), when the inclinometer was tilted towards 45° between +x+y axis (with reference to the scheme shown in Fig. 3(c)), from 0° - 90° , a simultaneous biaxial response from the gratings on the +x side and +y sides could be observed. Further, as the inclinometer is tilted towards 45° between the -x-y axis (again with reference to Fig. 3(c)), a similar pattern in the simultaneous biaxial response was observed, as shown in this case in Fig. 8(b). Similar to Fig. 6, the response of tilt sensor T1 were illustrated in greater details in each subplot of Fig. 8.

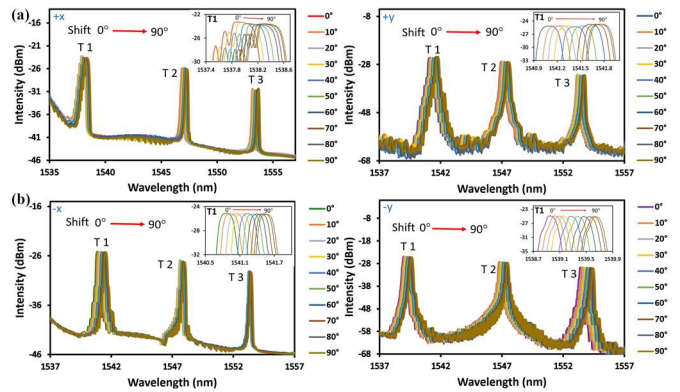


Fig. 8. Shifts of the wavelength spectra for each tilt sensor T1, T2 and T3 as the inclinometer is tilted from 0° to 90° towards 45° between the (a) +x and +y direction and (b) -x and -y direction at room temperature (27°C). (insets: illustrate the expanded version of tilt sensor T1 to clearly indicate the shift, as an example.)

These positive results have shown very clearly that the inclinometer could operate successfully over the tilt range from 0° to 90° , on any direction, as it is clear that a tilt in any direction will cause a shift in the spectrum of the FBG-based sensor, used to monitor that specific axis.

Fig. 9 shows the calibration of the tilt sensor T1, as it is tilted from 0° to 90° towards (a) +x, (b) -x, (c) +y, and (d) -y

directions. A linear relationship between the tilt angle and the wavelength shifts is observed, with a sensitivity of 0.008 nm (+x), 0.013nm (-x), 0.012 nm (+y), and 0.011 nm (-y) per degree of inclination. Thus, the average sensitivity of the FBG is 0.01 nm per degree of inclination. The graphs were obtained from three different readings when the inclinometer is tilted

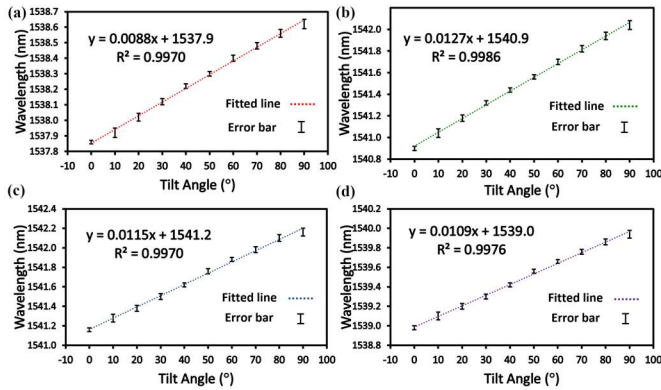


Fig. 9. Illustrations of wavelength over tilt angle with error bars for tilt sensor T1, as it is tilted from 0° to 90° towards (a) +x, (b) -x, (c) +y, and (d) -y directions at room temperature (27°C).

towards the specified axis mentioned. From the error bars, it can be seen that the deviation is small hence the linear response is verified.

During the tilt towards the direction of 20°, 45°, and 70° between +x and +y axis, a similar linear relationship between the wavelength shift and the inclination angle, was also obtained. A comparison of the sensitivity for tilt sensor T1 between a tilt along the axis +x and +y) and a tilt of 20°, 45°, and 70° from the respective axis (+x and +y) was made. In this case, the FBG's response at the +x and +y side during a single axis tilt (refer to Fig. 9(a) and (c)) is compared to the response of the same grating during biaxial tilts. The results are illustrated in Fig. 10(a) and (b) for the +x and +y sides, respectively. From these figures, the wavelength shifts of the grating at tilt sensor (T1) during the single-axis tilt (+x and +y)

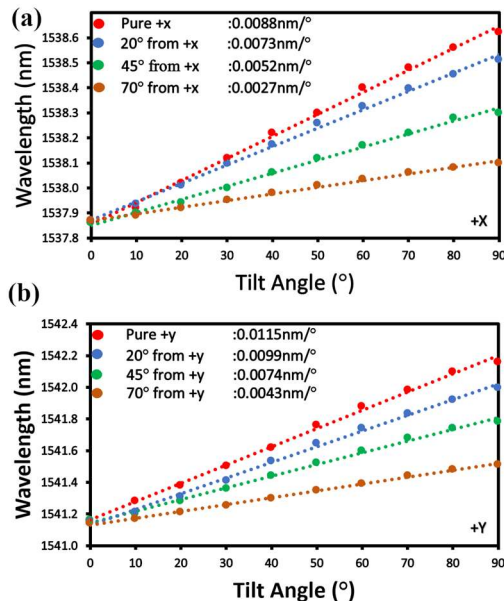


Fig. 10. The linear response of the gratings at the (a) +x side and (b) +y side for tilt sensor T1, during the tilt towards the respective axis (pure +x and pure +y), and also 20°, 45°, and 70° from the axis, at room temperature (27°C).

are greater than the 20°, 45°, 70° biaxial tilt. This is simply because, during the biaxial tilts, both gratings along the +x axis and +y axes share the total downward force, resulting in a smaller net force to each of them. Hence, a lesser strain was applied to each grating in the tilt sensor, thus producing a smaller shift in the wavelength spectrum, as compared to the result from the single-axis tilt.

Besides that, Fig. 10 shows that the sensors exhibit different force decomposition between two axes. The figure clearly illustrates different sensitivities for a tilt at different angles between the two axes. During the tilt towards 20° from +x (70° from +y), the grating facing +x has a higher sensitivity of 0.0073nm/° compared to the grating facing +y with a sensitivity of 0.0043nm/°. We could see a similar pattern during the tilt towards 20° from +y (70° from +x), where the FBG facing +y exhibit higher sensitivity of 0.0099nm/° compared to FBG facing +x with a sensitivity of 0.0027nm/°. From the sensitivity of the gratings, during the tilt 20° from +x (70° from +y), it can be deduced that the FBGs facing +x direction exhibits greater wavelength shifts compared to the FBGs facing +y as gratings closer to the tilt axis experience greater downward force, causing greater strain to the FBG and vice versa.

Fig. 11 illustrates (a) the shift in the reflected peak spectrum of FBG T (which is insensitive to strain) due to the change in temperature, over the range from -25°C to 80°C and (b) the shift in the peak spectrum of this grating, FBG T, showing its linear response due to the change in temperature over the range from -25°C to 80°C. To ensure that it does provide the temperature compensation needed, the FBG was exposed to the extreme range of temperatures that would be expected in field use, thus calibrating over the range -25°C to 80°C. A linear response to temperature, with a sensitivity of 0.011nm/°C, indicates that a simple temperature compensation approach can be applied to the inclinometer to allow correction for any temperature

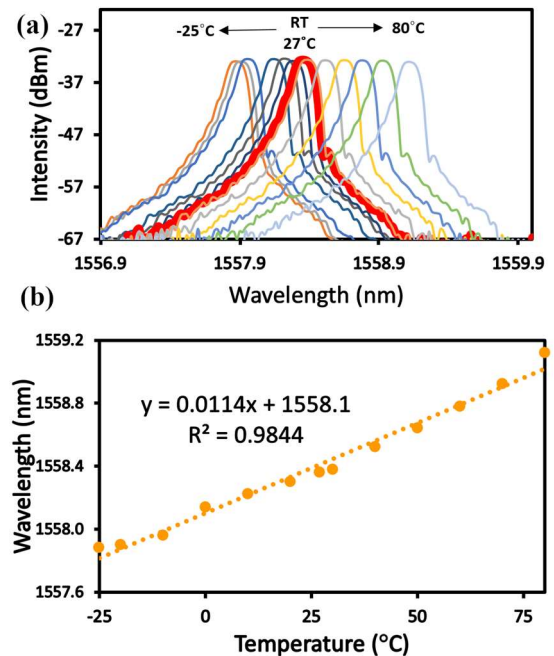


Fig. 11. Illustrations of (a) shift in the reflected peak spectrum of FBG T (insensitive to strain) due to the change in temperature over the range from -25°C → 80°C (RT – room temperature of 27°C) and (b) shift in the peak spectrum of FBG T showing a linear response due to the change in temperature over the range from -25°C → 80°C.

changes that occur during the operation of the device in-the-field, for example from night to day temperatures.

IV. CONCLUSION

A practical and compact FBG-based inclinometer has been designed, fabricated and evaluated. This has been based on 3D-printed biaxial tilt sensors utilizing four FBGs to ensure biaxial measurements. The experimental results showed an excellent degree of linearity in the response, not only of each FBG over a range of inclination angle of 0° to 90° (with an average sensitivity of 0.01nm per inclination degree) but of the system as a whole. The inclinometer further has been designed to operate over a wide temperature range, such as would be experienced in-the-field by including a facility for temperature compensation (through a strain-insensitive FBG that provides a temperature compensation factor of 0.01nm/°C). The inclinometer has the ability not only to measure biaxial response, but also at 45° between the inclination axis, showing a wider dimension to the inclination measurement possible.

The device is compact and inexpensive to produce, as well as being designed for use outside the laboratory. There, the ability of this inclinometer to operate in two axes, at extreme temperatures (-25°C to 80°C), opens up potential applications in civil engineering, especially in slope and structural monitoring and in the protection of vulnerable communities affected by landslips after major weather events.

ACKNOWLEDGMENT

K. T. V. Grattan acknowledges support from the Royal Academy of Engineering.

REFERENCES

- [1] P. Ferdinand, S. Magne, V. Dewynter-Marty, S. Rougeault, and L. Maurin, "Applications of Fiber Bragg Grating sensors in the composite industry," *MRS Bull.*, vol. 27, no. 5, pp. 400–407, 2002, doi: <https://doi.org/10.1557/mrs2002.126>.
- [2] Y.-T. Ho, A.-B. Huang, J. Ma, and B. Zhang, "Ground movement monitoring using an optic fiber Bragg grating sensored system," *17th Int. Conf. Opt. Fibre Sensors*, vol. 5855, p. 1020, 2005, doi: [10.1117/12.623596](https://doi.org/10.1117/12.623596).
- [3] J. Dunicliff, "National Cooperative Highway Research Program Geotechnical Instrumentation for," no. April 1982, 1982.
- [4] G. Machan and V. G. Bennett, "Use of Inclinometers for Geotechnical Instrumentation on Transportation Projects," *Use Incl. Geotech. Instrum. Transp. Proj.*, no. October, 2008, doi: [10.17226/23074](https://doi.org/10.17226/23074).
- [5] Z. Mihalinc, M. Bačić, and M. S. Kovačević, "Risk identification in landslide monitoring," *Gradjevinar*, vol. 65, no. 6, pp. 523–536, 2013, doi: [10.14256/jce.717.2012](https://doi.org/10.14256/jce.717.2012).
- [6] R. Olaru and C. Cotae, "Tilt sensor with magnetic liquid," *Sensors Actuators, A Phys.*, vol. 59, no. 1–3, pp. 133–135, 1997, doi: [10.1016/S0924-4247\(97\)80162-8](https://doi.org/10.1016/S0924-4247(97)80162-8).
- [7] M. Drahanaky, "Liveness Detection in Biometrics," in *Advanced Biometric Technologies*, G. Chetty and J. Yang, Eds. Rijeka: IntechOpen, 2011.
- [8] Y. Yang, X. Ma, K. Chen, E. Wang, Z. Yu, and Q. Yu, "A high-resolution dynamic fiber-optic inclinometer," *Sensors Actuators, A Phys.*, vol. 283, pp. 305–312, 2018, doi: [10.1016/j.sna.2018.10.007](https://doi.org/10.1016/j.sna.2018.10.007).
- [9] L. M. N. Amaral, O. Frazão, J. L. Santos, and A. B. Lobo Ribeiro, "Fiber-optic inclinometer based on taper Michelson interferometer," *IEEE Sens. J.*, vol. 11, no. 9, pp. 1811–1814, 2011, doi: [10.1109/JSEN.2011.2105264](https://doi.org/10.1109/JSEN.2011.2105264).

- [10] M. F. Ghazali, H. Mohamad, and K. A. Ang, "Development of distributed fibre optic inclinometer for landslide and geotechnical application," in *16th Asian Regional Conference on Soil Mechanics and Geotechnical Engineering, ARC 2019*, 2020, pp. 3–6.
- [11] L. Schenato *et al.*, "Distributed optical fibre sensing for early detection of shallow landslides triggering," *Sci. Rep.*, vol. 7, no. 1, pp. 1–7, 2017, doi: [10.1038/s41598-017-12610-1](https://doi.org/10.1038/s41598-017-12610-1).
- [12] M. Maheshwari, Y. Yang, D. Upadrashta, and T. Chaturvedi, "A Rotation Independent In-Place Inclinometer/Tilt Sensor Based on Fiber Bragg Grating," *IEEE Trans. Instrum. Meas.*, vol. 68, no. 8, pp. 2943–2953, 2019, doi: [10.1109/TIM.2018.2870246](https://doi.org/10.1109/TIM.2018.2870246).
- [13] C. Hong, Y. Zhang, Z. Lu, and Z. Yin, "A FBG Tilt Sensor Fabricated Using 3D Printing Technique for Monitoring Ground Movement," *IEEE Sens. J.*, vol. 19, no. 15, pp. 6392–6399, 2019, doi: [10.1109/JSEN.2019.2908873](https://doi.org/10.1109/JSEN.2019.2908873).
- [14] S. He, X. Dong, K. Ni, Y. Jin, C. C. Chan, and P. Shum, "Temperature-insensitive 2D tilt sensor with three fiber bragg gratings," *Meas. Sci. Technol.*, vol. 21, no. 2, 2010, doi: [10.1088/0957-0233/21/2/025203](https://doi.org/10.1088/0957-0233/21/2/025203).
- [15] H. Y. Au, S. K. Khijwania, H. Y. Fu, W. H. Chung, and H. Y. Tam, "Temperature-insensitive fiber bragg grating based Tilt sensor with large dynamic range," *J. Light. Technol.*, vol. 29, no. 11, pp. 1714–1720, 2011, doi: [10.1109/JLT.2011.2132695](https://doi.org/10.1109/JLT.2011.2132695).
- [16] H. Bao, X. Dong, L. Y. Shao, C. L. Zhao, and S. Jin, "Temperature-insensitive 2-D tilt sensor by incorporating fiber Bragg gratings with a hybrid pendulum," *Opt. Commun.*, vol. 283, no. 24, pp. 5021–5024, 2010, doi: [10.1016/j.optcom.2010.07.050](https://doi.org/10.1016/j.optcom.2010.07.050).
- [17] X. Dong, L. Hu, L. Shao, Y. Wang, and J. Zheng, "Temperature-insensitive 2D fiber Bragg grating TILT sensor," *Microw. Opt. Technol. Lett.*, vol. 55, no. 2, pp. 344–346, 2013, doi: [10.1002/mop.27281](https://doi.org/10.1002/mop.27281).
- [18] Y. L. Wang, B. Shi, T. L. Zhang, H. H. Zhu, Q. Jie, and Q. Sun, "Introduction to an FBG-based inclinometer and its application to landslide monitoring," *J. Civ. Struct. Heal. Monit.*, vol. 5, no. 5, pp. 645–653, 2015, doi: [10.1007/s13349-015-0129-4](https://doi.org/10.1007/s13349-015-0129-4).
- [19] K. Ni, X. Dong, Y. Jin, and H. Xu, "Temperature-independent fiber bragg grating tilt sensor," *Microw. Opt. Technol. Lett.*, vol. 52, no. 10, pp. 2250–2252, 2010, doi: [10.1002/mop.25425](https://doi.org/10.1002/mop.25425).
- [20] K. O. Hill and G. Meltz, "Fiber Bragg Grating Technology Fundamentals and Overview," *J. Light. Technol.*, vol. 15, no. 8, pp. 1263–1276, 1997, doi: <https://doi.org/10.1109/50.618320>.
- [21] A. D. Kersey *et al.*, "Fiber grating sensors," *J. Light. Technol.*, vol. 15, no. 8, pp. 1442–1462, 1997, doi: [10.1109/50.618377](https://doi.org/10.1109/50.618377).
- [22] H. Bao, X. Dong, C. Zhao, L. Y. Shao, C. C. Chan, and P. Shum, "Temperature-insensitive FBG tilt sensor with a large measurement range," *Opt. Commun.*, vol. 283, no. 6, pp. 968–970, 2010, doi: [10.1016/j.optcom.2009.11.014](https://doi.org/10.1016/j.optcom.2009.11.014).
- [23] X. Dong, C. Zhan, K. Hu, P. Shum, and C. C. Chan, "Temperature-insensitive tilt sensor with strain-chirped fiber Bragg gratings," *IEEE Photonics Technol. Lett.*, vol. 17, no. 11, pp. 2394–2396, 2005, doi: [10.1109/LPT.2005.857978](https://doi.org/10.1109/LPT.2005.857978).



N. N. Ismail received the Bachelor of Engineering (Hons) Electronics (Communication) from the Faculty of Electrical Engineering, Universiti Teknologi MARA in 2012. She received her Ph.D. degree from the Faculty of Electrical Engineering, UiTM Shah Alam by a fast-track program in 2018. She has been a Post-Doctoral Research Fellow with the Photonics Research Centre, University of Malaya, since 2019. Her research interests include saturable absorbers and high-power laser.



M. S. M. Sa'ad received the Bachelor of Science (Hons) in Pure Physics from the Faculty of Science, University of Malaya in 2019. He is currently a postgraduate student and a research assistant at the Photonics Research Centre, University of Malaya. His research interest focuses on fiber optic sensors mainly on fiber Bragg gratings.



M. F. Ismail obtained his Bachelor of Engineering (Telecommunication) from the Faculty of Engineering, University of Malaya in 1999 and Master of Engineering (Science) from the Faculty of Engineering, University of Malaya in 2004. His research focuses on pulsed, multiwavelength fibre lasers and waveguide.



M. K. A. Zaini received the bachelor's degree from the Department of Physics, Faculty of Science, University Putra Malaysia, Malaysia, in 2015, and currently a postgraduate candidate at Photonics Research Centre, University of Malaya. His current research interest includes fiber Bragg grating sensors, and Spatial Division Multiplexing.



K. S. Lim (M'16) received the B.E. degree from the Department of Electrical Engineering, Faculty of Engineering, University of Malaya, Malaysia, in 2008, and the Ph.D. degree from the Photonics Research Centre, Department of Physics, University of Malaya, in 2012. He is currently a Senior Lecturer with the Photonics Research Centre, University of Malaya. His current research interests include fiber Bragg grating sensors, spatial division multiplexing, and laser medical devices. He is a Corporate Member of the Institute of Engineers Malaysia (IEM), a registered Professional Engineer (Telecommunication) of the Board of Engineers Malaysia (BEM), and a member of OSA.



K. T. V. Grattan graduated in Physics from Queen's University Belfast with a BSc (First Class Honours) in 1974, followed by a PhD in Laser Physics. His doctoral research involved the use of laser-probe techniques for measurements on potential new laser systems. He obtained the degree of Doctor of Science (DSc) from City University in 1992 for his sensor work. His research interests have expanded to include the development and use of fibre optic and optical systems in the measurement of a range of physical and chemical parameters.



G. Brambilla is a professor at the Optoelectronics Research Centre and, since 2016, co-Director and General Manager of the Future Photonics Hub. He has been Director of the Centre for Innovative Manufacturing in Photonics until 2015. He obtained his MSc (Engineering) with honours from Politecnico di Milano (Italy) in 1996 and his PhD degree in Optoelectronics from the University of Southampton in 2002. In 2007 he was awarded the Royal Society Research Fellowship, which was then extended in 2012. His research interests include optical fibre sensors; optical fibre structuring using fs lasers; specialty and polymer fibres; new fibre fabrication technologies; UV fibre lasers; devices based on optical fibre nanowires, fibre tapers and couplers; rare earth doped scintillating fibres and fibres for nuclear sensing.



B. M. A. Rahman received BSc Eng and MSc Eng degrees in Electrical Engineering with distinctions from Bangladesh University of Engineering and Technology (BUET), Dhaka, Bangladesh, in 1976 and 1979, respectively. He received his PhD degree in Electronic Engineering from University College, London in 1982. From 1976 to 1979, he was a Lecturer at the Electrical Engineering Department, BUET. In 1988, he joined the Electrical, Electronic and Information Engineering Department of City University, London, as a Lecturer, where he is now a Professor. At City University, he leads the research group on Photonics Modelling, specialised in the development and use of the rigorous and full-vectorial numerical approaches, frequency domain modal solution approach, the beam propagation method, and time-domain approach, primarily based on the numerically efficient finite element method.



H. Mohamad is an Associate Professor at Universiti Teknologi PETRONAS. He holds BEng in Civil Engineering from Universiti Teknologi Malaysia, MSc in Soil Mechanics from Imperial College London and PhD in Geotechnical Engineering from University of Cambridge. Dr Mohamad specializes in the area of Geotechnical Engineering and an expert in fibre-optic distributed sensing. Some of his notable involvements of construction monitoring projects using innovative fibre-optic sensing include monitoring tunnel deformation at London King's Cross and Singapore's Mass Rapid Transport (MRT) Circle Line. In 2013, Hisham joined Geotechnics Division, Ministry of Mobility and Public Works in Belgium for a year and was involved in monitoring ground excavation and construction projects of the world's largest shipping lock in Antwerp.



H. Ahmad received the Ph.D. degree in laser technology from the University of Wales, Swansea, U.K., in 1983. He is currently a Professor with the Department of Physics and director of the Photonics Research Centre, University of Malaya, Kuala Lumpur, Malaysia, where he has actively pursued research activities in the field of photonics since 1983. He is the author of more than 400 professional papers in international journals and conference proceedings. His research interests are in lasers, fiber-based devices for telecommunications, and fiber-based sensor devices. Dr. Ahmad is a Fellow of the Academy of Sciences, Malaysia.